Available online at www.sciencedirect.com
ScienceDirect
Trans. Nonferrous Met. Soc. China 24(2014) 2752−2760
Transactions of Nonferrous Metals Society of China
www.tnmsc.cn

Effect of Sr content on microstructure and mechanical properties of Mg−Li−Al−Mn alloy

Tian-cai XU[1], Xiao-dong PENG[1,2], Jun-wei JIANG[1], Wei-dong XIE[1,2], Yuan-fang CHEN[1,3], Guo-bing WEI[1]

1. College of Materials Science and Engineering, Chongqing University, Chongqing 400044, China;
2. National Engineering Research Center for Magnesium Alloys, Chongqing University, Chongqing 400044, China;
3. College of Materials Science and Engineering, Chongqing University of Technology, Chongqing 400050, China

Received 8 August 2013; accepted 6 January 2014

Abstract: The as-cast Mg−8Li−3Al−0.5Mn−*x*Sr (LAM830−*x*Sr, *x*=0−1.0) alloys were designed and prepared in a vacuum induction furnace under controlled argon atmosphere. The alloys were then processed by hot extrusion, and their microstructural evolution and mechanical properties were analyzed. Results indicate that the LAM830 alloy mainly consists of α-Mg, β-Li, Al_2Mn_3, and $LiMgAl_2$ phases. Sr addition results in the precipitation of Al−Sr. Moreover, Sr addition results in a fact that the secondary dendrite arm spacing (DAS) of the primary α-Mg phase is obvious refined. Microstructure of the investigated alloys is further refined as a result of the hot extrusion treatment. The content and morphology of the secondary phases have important effects on the mechanical properties of the alloys. The as-extruded LAM830−0.5Sr alloy exhibits an optimal elongation of 22.43% and as-extruded LAM830−0.75Sr alloy shows an optimal tensile strength of 265.46 MPa.

Key words: Mg−Li alloy; dendrite arm spacing; Al_4Sr phase; mechanical properties

1 Introduction

Lightweight structural materials are recently drawing increased attention of researchers and engineers as potential candidates for improving the fuel efficiency and reducing the greenhouse gas emissions in the transportation industry [1,2]. Among them, Mg–Li alloys are considered to be the lightest structural materials with low density (1.3−1.6 g/cm^3), high specific stiffness, good machining property, good damping capacity, and excellent formability [3]. Owing to these advantageous properties, Mg−Li alloys have been extensively used in the fields such as spaceflight and weapon industry. The binary phase diagram of the Mg−Li system shows that the Li content in the alloy is a key factor affecting the microstructure and properties of this series of alloys. The Mg−Li phase diagram indicates that when mass fraction of Li ranges from 5.7% to 10.3%, a duplex alloy is formed containing both HCP-structured α-Mg phase and BCC-structured β-Li phase which is a Li solid solution formed by Mg dissolving in Li. In the case of the HCP α-Mg phase, the Li addition leads to the reduction of c/a axial ratio of the HCP lattice such that the sliding systems are easy to activate. The BCC β-Li phase has more active slip systems than the HCP phase. Therefore, the ductility of Mg−Li alloy is better than that of traditional Mg alloys [4,5].

Despite the advantageous properties, the wide applicability of Mg−Li alloys is still restricted due to inherent limitations, such as age hardening stability, low tensile strength, and poor corrosion resistance [6]. It is well known that the formability and associated properties of Mg alloys can be improved via alloying with metals, such as Al, Mn, and Sr [7]. This process of alloying is expected to improve the mechanical properties of Mg alloys through grain refining, solid-solution strengthening, and secondary phase strengthening [8]. For instance, it was reported that the addition of Mn transforms Fe and certain other impurities in the alloy to relatively harmless intermetallic compounds. Furthermore, Mn addition contributes to grain refinement and high formability during extrusion [9−11]. As a representative alkaline-earth element, Sr has also been

Foundation item: Project (2007CB613702) supported by the National Basic Research Program of China; Project (2008BB4323) supported by the Natural Science Foundation of Chongqing Science and Technology Commission, China; Project (2010DFR50010) supported by the International Scientific and Technological Cooperation Projects, China
Corresponding author: Xiao-dong PENG; Tel/Fax: +86-23-65111625; E-mail: pxd@cqu.edu.cn
DOI: 10.1016/S1003-6326(14)63406-3

considered for alloying with Mg alloys. Recently, several studies have demonstrated the industrial use of Sr, especially for the modification of Al−Si alloys [12]. These results suggest the potential use of Sr as an additive for realizing grain refinement in Mg−Al alloy series [13].

Therefore, in this study, the effects of Sr addition on the microstructure and mechanical properties of the as-cast and as-extruded Mg−8Li−3Al−0.5Mn alloy were investigated.

2 Experimental

The alloy was prepared using pure ingots (purity 99.9%) of Mg, Li and Al. Master alloys were prepared in the composition of Mg−5%Mn and Mg−10%Sr (mass fraction), which contained Mn and Sr, respectively. The materials were first loaded in a graphite crucible, which was mounted in a vacuum induction furnace. Subsequently, the furnace chamber was evacuated and maintained at the pressure of 1×10^{-1} Pa. Prior to melting, Ar gas was introduced into the chamber and maintained at standard atmospheric pressure during melting. The melt was maintained for 30 min at 700 °C, without stirring the mixture. Following that, the melt was cast in a permanent mold with dimensions of 90 mm×300 mm, which was preheated to the temperature of 220 °C. Following that, the homogenization treatment was conducted in the vacuum furnace for 6 h at 240 °C. For the homogenization treatment, the furnace chamber was evacuated to 1×10^{-1} Pa, with the supply of Ar at atmospheric pressure during the homogenization. The specimens were extruded at 300 °C from *d*80 mm to *d*16 mm, with extrusion ratio of 25 and at extrusion speed of 10 mm/s. The chemical composition of the as-cast alloys was determined by inductively coupled plasma atomic emission spectroscopy (ICP-AES). The corresponding results are listed in Table 1.

Table 1 Actual chemical compositions of experimental alloys (mass fraction, %)

Alloy	Li	Al	Mn	Sr	Mg
Mg−8Li−3Al−0.5Mn	8.20	2.93	0.49	−	Bal.
Mg−8Li−3Al−0.5Mn−0.25Sr	8.36	3.02	0.58	0.28	Bal.
Mg−8Li−3Al−0.5Mn−0.5Sr	8.25	3.23	0.53	0.49	Bal.
Mg−8Li−3Al−0.5Mn−0.75Sr	8.09	3.18	0.62	0.76	Bal.
Mg−8Li−3Al−0.5Mn−1.0Sr	8.12	2.98	0.42	1.13	Bal.

Furthermore, tensile tests of the alloys were conducted at ambient temperature on an electro-universal testing machine (Instron 5569) with the crosshead speed of 1.5 mm/min. The metallographic specimens were cut from the same position after each casting and extruding step. The cut specimens were polished and etched in 8% nitric acid solution in distilled water and the solution of 1.5 g picric, 25 mL ethanol, 5 mL acetic acid and 10 mL distilled water, respectively. The obtained specimens were analyzed by optical microscopy (Olympus) and scanning electron microscopy (SEM, JOEL/JSM-6460LV) equipped with energy-dispersive X-ray spectroscope (EDS, Oxford). In addition, the crystalline phase of the specimens was identified by X-ray diffraction (XRD, D/MAX-A).

3 Results

3.1 Microstructure

Figure 1 shows the microstructure of the as-cast alloys. Since the Li content in the prepared alloys is 8%, these alloys contain both white α-Mg phase and black β-Li phase. The formation of dendritic α-Mg phase is observed in the SEM image, as shown in Fig. 1(a). Moreover, Sr addition results in a fact that the secondary dendrite arm spacing of the primary α-Mg phase is obvious refined. Figure 1(b) shows the microstructure of LAM830−0.25Sr alloy. As seen from the figure, Sr addition results in the replacement of the long-striped α-Mg phase with a blocky structure. As Sr content increases to 0.5%, Sr addition strengthens the refining effect. The blocky structure of α-Mg phase becomes smaller, exhibiting a uniform distribution. Meanwhile, the formation of a new intermetallic compound distributes along the phase boundaries between α-Mg and β-Li phases with discontinuous network morphology. This phenomenon becomes increasingly evident with the increase of Sr content. As shown in Fig. 1(d), numerous new blocky intermetallic compounds are formed around the irregular-shaped α-Mg phase. However, when the Sr content increases to 1.0%, the change in α-Mg phase is not observed, and the blocky intermetallic compound segregates at the β-Li phase grain boundaries.

Figure 2 shows the XRD patterns of the as-cast alloys. It is obvious that the diffraction patterns of LAM830 alloy mainly contain α-Mg, β-Li matrix, and Al_2Mn_3 and $LiMgAl_2$ phases. Here, $MgLiAl_2$ phase is stable at room temperature and is formed by the transformation of metastable Li_2MgAl phase [14]. However, with the addition of Sr, additional peaks correspond to the Al_4Sr, Mg_2Sr and Mn phases. Furthermore, the Mg_2Sr and Mn peaks intensities gradually increase with the increase of Sr content. The contrast tomography indicates significant broadening of the weak diffraction patterns of Mg_2Sr and Mn precipitated in the LAM830−0.75Sr and LAM830−1.0Sr alloys.

Furthermore, the LAM830−*x*Sr (*x*=0, 0.5, 0.75, 1.0) alloys were characterized via SEM equipped with EDS and computer-controlled imaging system. The SEM

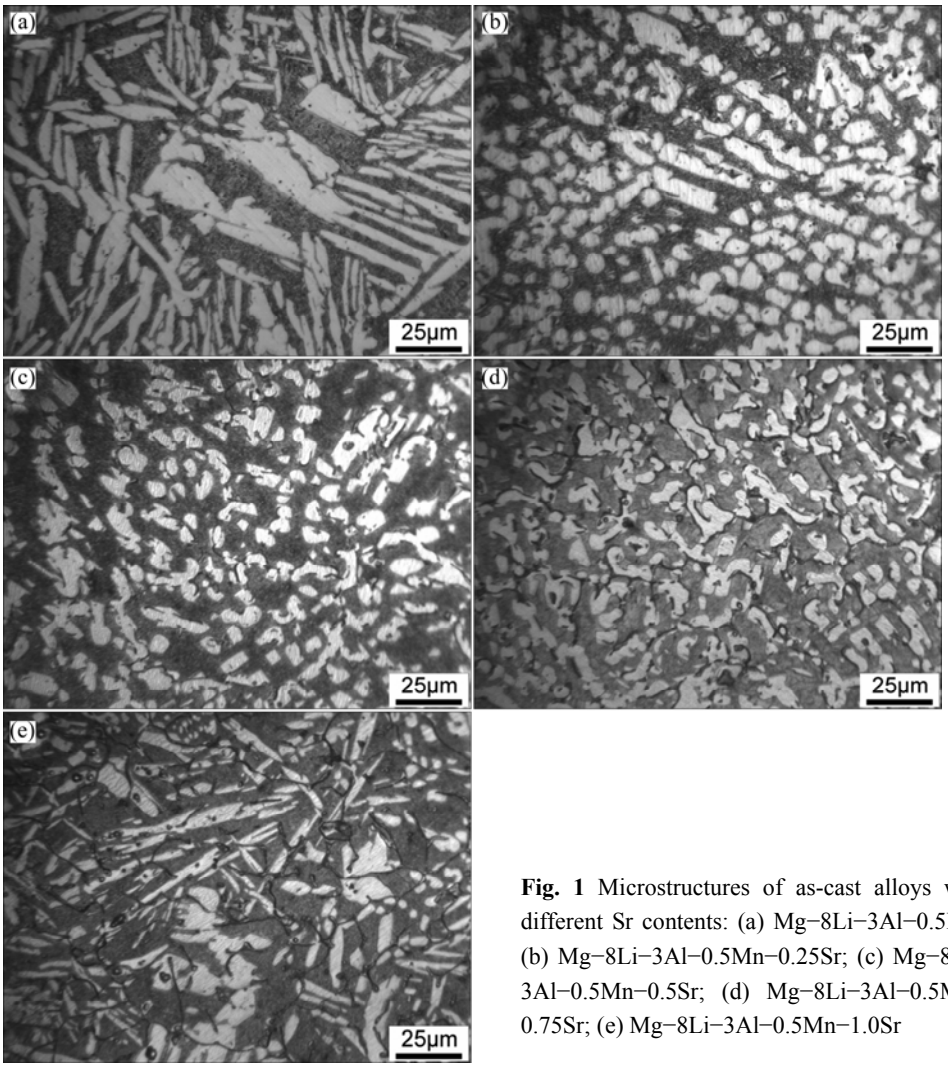

Fig. 1 Microstructures of as-cast alloys with different Sr contents: (a) Mg−8Li−3Al−0.5Mn; (b) Mg−8Li−3Al−0.5Mn−0.25Sr; (c) Mg−8Li−3Al−0.5Mn−0.5Sr; (d) Mg−8Li−3Al−0.5Mn−0.75Sr; (e) Mg−8Li−3Al−0.5Mn−1.0Sr

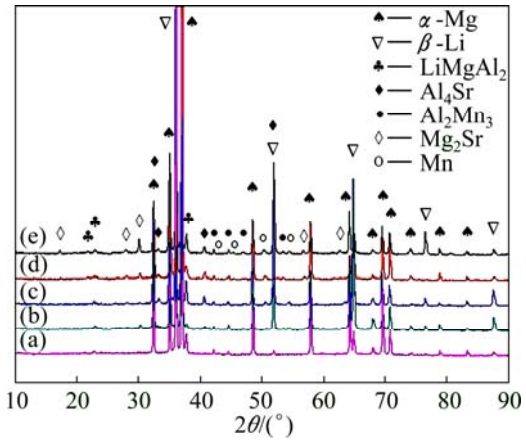

Fig. 2 XRD patterns of different alloys: (a) Mg−8Li−3Al−0.5Mn; (b) Mg−8Li−3Al−0.5Mn−0.25Sr; (c) Mg−8Li−3Al−0.5Mn−0.5Sr; (d) Mg−8Li−3Al−0.5Mn−0.75Sr; (e) Mg−8Li−3Al−0.5Mn−1.0Sr

images of the as-cast LAM830 alloy indicate dark and gray areas corresponding to α-Mg phase and β-Li phase, respectively, as shown in Fig. 3(a). The granular particles of the intermetallic compounds are randomly distributed in the α-Mg and β-Li matrixes. From Fig. 3(b), quantitative EDS analysis indicates that the mole ratio of Al to Mn at location *A* is approximately 2:3. According to the XRD results reported earlier, it is concluded that the granular particles of intermetallic compounds are Al_2Mn_3. Figures 3(c) and (d) show the SEM images and EDS point analysis of the as-cast LAM830–0.5Sr alloy, respectively. It indicates the formation of new intermetallic compound with fishbone-like morphology, which is distributed in the α-Mg and β-Li matrixes. EDS point analysis, which was performed at location *B*, indicates the presence of Mg, Al and Sr. The corresponding mole ratio of Al to Sr is estimated to be 4:1. According to the XRD results, these compounds may comprise Al_4Sr.

Figures 3(e) and (f) show the SEM images of the LAM830−0.75Sr and LAM830−1.0Sr alloys, respectively. The corresponding results of micro-area chemical composition analysis are listed in Table 2. The EDS point analysis, which was performed at specific

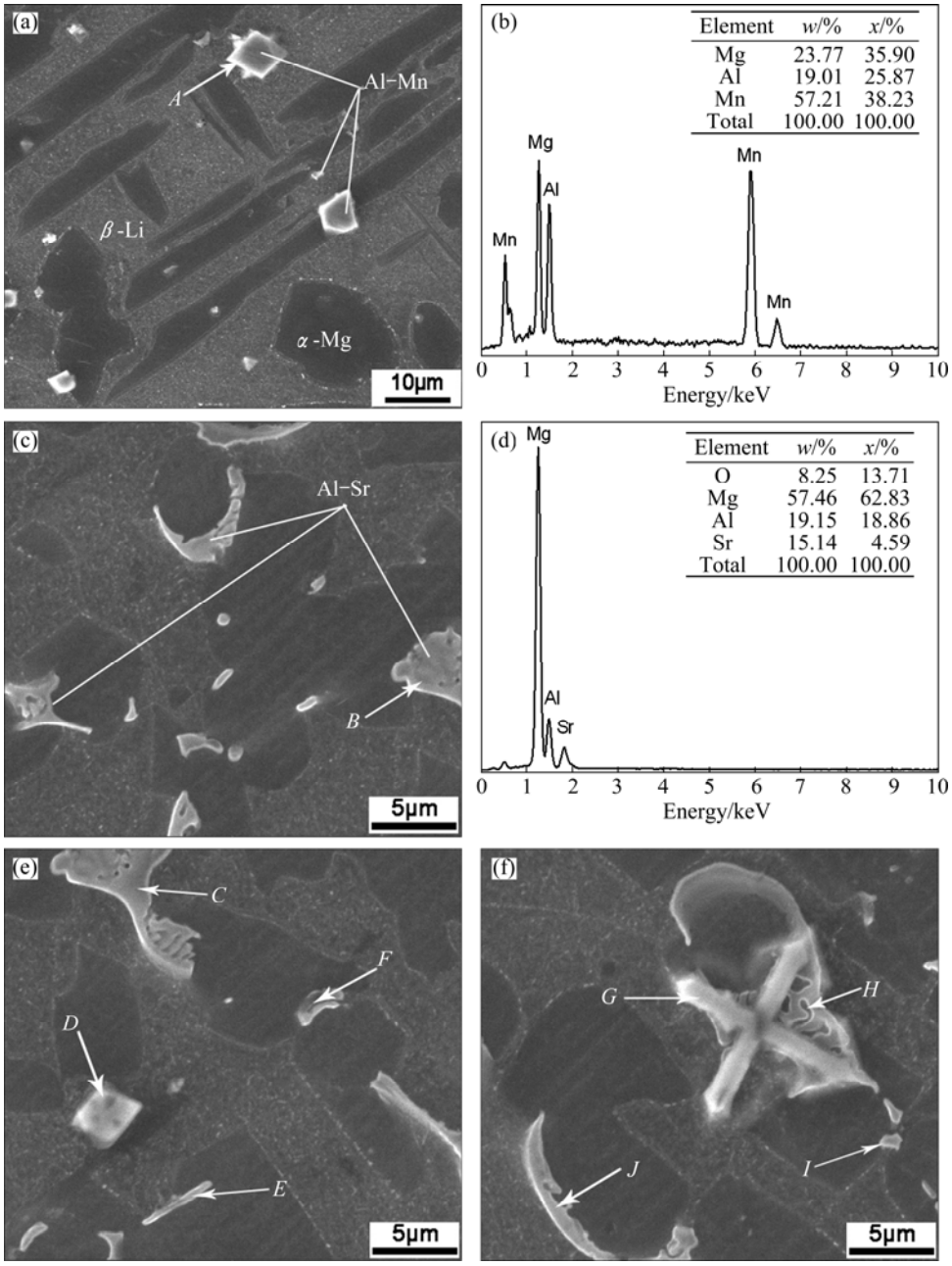

Fig. 3 SEM images and EDS analysis for Mg−8Li−3Al−0.5Mn alloy (a, b), Mg−8Li−3Al−0.5Mn−0.5Sr alloy (c, d), Mg−8Li−3Al−0.5Mn−0.75Sr alloy (e), Mg−8Li−3Al−0.5Mn−1.0Sr alloy (f)

Table 2 Element contents of different positions in Fig. 3 (mole fraction, %)

Position	O	Mg	Al	Mn	Sr
C	10.40	70.33	15.03	−	4.24
D	19.22	25.78	22.17	32.83	−
E	19.79	75.25	−	−	4.96
F	26.58	66.69	−	−	6.73
G	15.26	69.34	6.49	8.91	−
H	10.93	76.61	8.62	−	3.84
I	29.16	69.02	−	−	1.82
J	15.14	69.68	11.76	−	3.42

locations labeled as *C*, *E*, *F*, *H*, *I*, and *J*, indicates the presence of Mg, Al and Sr. According to the XRD results, these compounds can be related to Al_4Sr and Mg_2Sr. Careful observation of locations *D* and *G* reveals that both these points consist of Al_2Mn_3 phase, although the shape and location are different. The Al_2Mn_3 phase and Al_4Sr phase present cross shape, while the single Al_2Mn_3 phase presents diamond shape. This could be directly related to the order of nucleation in the intermetallic compounds.

Figures 4 and 5 show the microstructures of the as-extruded alloys. It can be seen that the microstructures in the extruded alloys are much finer than those in the

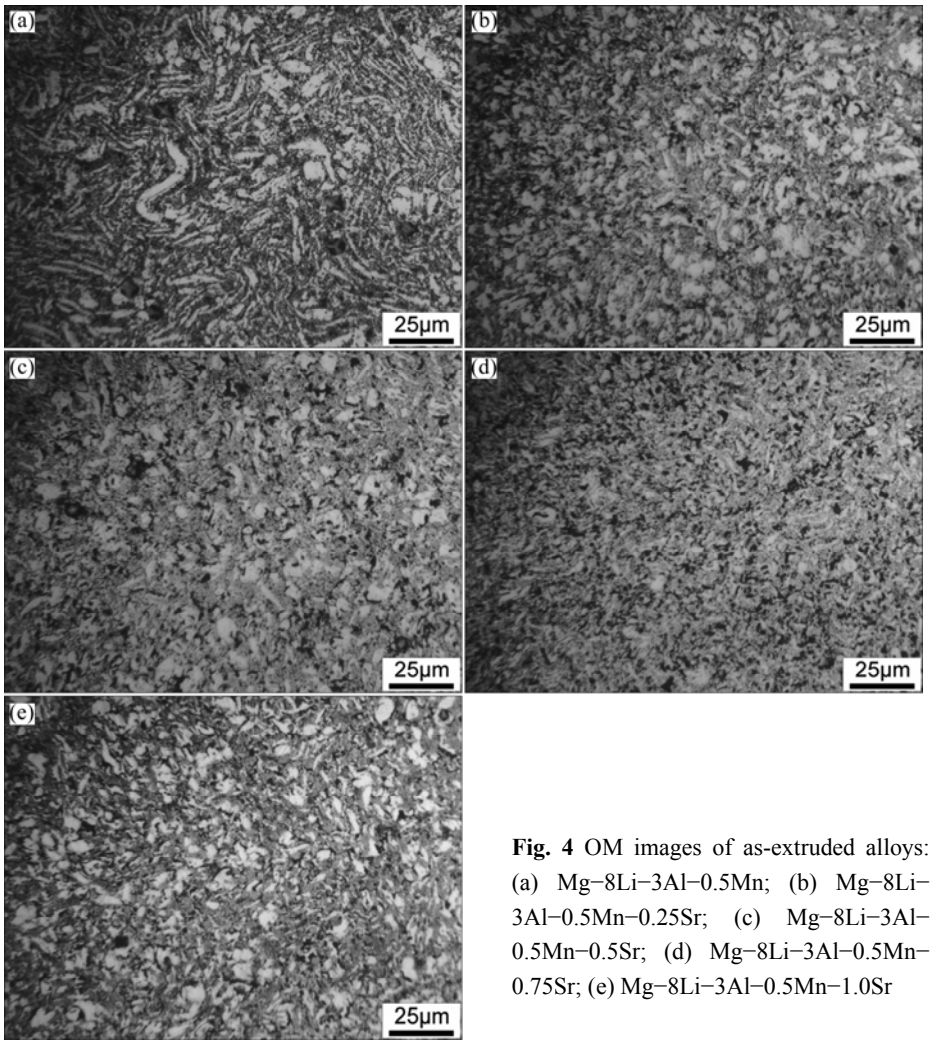

Fig. 4 OM images of as-extruded alloys: (a) Mg−8Li−3Al−0.5Mn; (b) Mg−8Li−3Al−0.5Mn−0.25Sr; (c) Mg−8Li−3Al−0.5Mn−0.5Sr; (d) Mg−8Li−3Al−0.5Mn−0.75Sr; (e) Mg−8Li−3Al−0.5Mn−1.0Sr

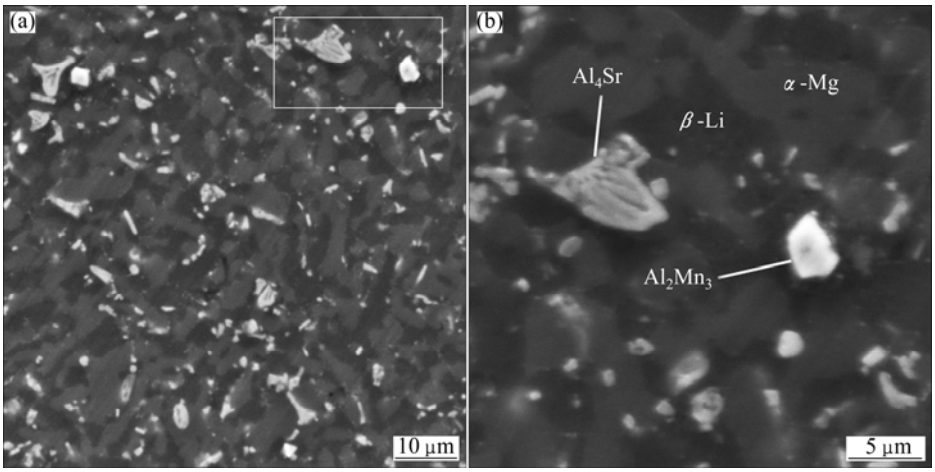

Fig. 5 SEM images of as-extruded Mg−8Li−3Al−0.5Mn−0.75Sr alloy: (a) Low magnification; (b) High magnification

corresponding as-cast alloys. As a result of the extrusion process (Fig. 4(a)), the shape of the α-Mg phase is transformed from long strip to curve under compression stress, while that of the β-Li phase is significantly refined. With the addition of Sr, the microstructure is refined further, and the LAM830−0.75Sr alloy exhibits the most refined microstructure. However, it is not uniform. This trend is similar to that observed in the as-cast alloys. The network of intermetallic compounds is crushed into small spherical particles, although the changes in granular Al_2Mn_3 intermetallic particles are not obvious during the hot extrusion.

Figure 5 shows the SEM images of the as-extruded LAM830−0.75Sr alloys. It can be seen that the α-Mg

phase in the extruded LAM830−0.75Sr alloy is much finer than the as-cast counterpart, and hence it is characterized as homogeneous and equiaxed. The α-Mg phase in the as-extruded alloy is 5−10 μm, whereas that of the corresponding as-cast α-Mg is 25−30 μm. Furthermore, as a result of extrusion, Al_4Sr with fishbone-like morphology and blocky Al_2Mn_3 compounds are crushed, which become granular and distribute depressively due to the dynamic recrystallization and extrusion stress during extrusion.

3.2 Mechanical properties

The mechanical properties of as-extruded alloys at room temperature are shown in Fig. 6 and Table 3. Results indicate that the tensile strength decreases to its lowest value with addition of 0.25% Sr. However, the tensile strength is significantly improved with addition of 0.75% Sr, at which the tensile strength reaches the peak value of 265.46 MPa. This value is 19.38% higher than the tensile strength of the LAM830 alloy without Sr. Further increase of Sr content results in the reduction of tensile strength. Furthermore, the elongation trend of alloys is observed to be different. The elongation trend is initially high and then decreases with the increase of Sr addition. When 0.5% Sr is added, the elongation reaches a peak value of 22.43% which increases by 43.97% compared with that of the alloy without Sr. However, the elongation of the alloys is found to decrease with further increase of Sr content.

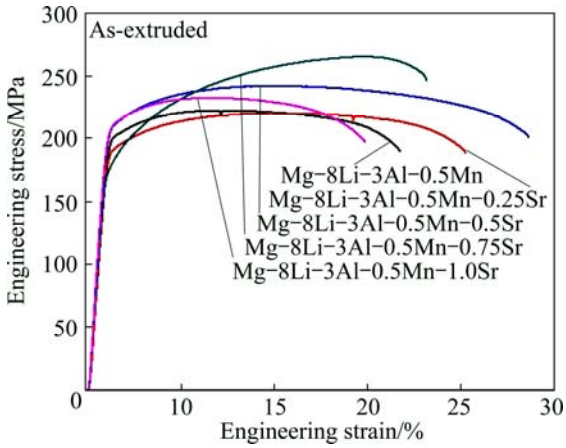

Fig. 6 Tensile stress−strain curves of as-extruded Mg−8Li−3Al−0.5Mn−xSr alloys at room temperature

Table 3 Tensile property of as-extruded Mg−8Li−3Al−0.5Mn−xSr alloys at room temperature

Alloy	Yield strenght/ MPa	Ultimate tensile strength/ MPa	Elongation/ %
Mg−8Li−3Al−0.5Mn	222.37	193.59	15.58
Mg−8Li−3Al−0.5Mn−0.25Sr	220.19	186.18	19.13
Mg−8Li−3Al−0.5Mn−0.5Sr	242.15	206.96	22.43
Mg−8Li−3Al−0.5Mn−0.75Sr	265.46	174.52	17.10
Mg−8Li−3Al−0.5Mn−1.0Sr	232.58	204.15	13.77

3.3 Fracture analysis

To gain further insights on the fracture mechanism in LAM830−xSr alloys, the fracture surface morphologies of the tensile specimens were examined using SEM. The fracture microstructure of the as-extruded LAM830 alloy indicates the formation of several dimples and some thin cleavage planes (Figs. 7(a, b)). This suggests that the fracture mechanism in LAM830 alloy is mainly attributed to ductile fracture and to some extent to the brittle fracture. The plate-like phases in the dimples are identified to be Al_2Mn_3 intermetallic compounds, as determined from the electron backscattered image and EDS analysis (Table 4). In addition, some cracks between the matrix and Al_2Mn_3 phase are observed. This illustrates that the cracks around Al_2Mn_3 phase are easily formed in LAM830 alloy under serious stress concentration.

However, with the addition of 0.5% Sr, the number of dimples on the fracture surfaces increases, while the secondary phase in the dimples is less than that in LAM830. The EDS point analysis performed at locations *C*, *D*, and *E* indicates the formation of Al_4Sr and Al_2Mn_3 (Figs. 7(c, d) and Table 4). No obvious crack is observed between the matrix and the Al_4Sr phase, suggesting that the matrix–Al_4Sr interface is strong. The microcracks between the matrix and secondary phase are not readily formed due to the fine secondary phases without serious stress concentration [15].

From Figs. 7(e, f), it can be found that the secondary phase partly assembles with addition of 1.0% Sr. Although dimples still exist on the fracture surfaces, the cracks exist around the secondary phase. This indicates that the secondary phase assembles partly, resulting in spots of stress concentration during tension test, leading to poor ductility.

4 Discussion

The microstructure of LAM830 alloy comprises α-Mg, β-Li, Al_2Mn_3, and $LiMgAl_2$ phases. Sr addition results in the formation of blocky intermetallic compounds with discontinuous network morphology. The XRD and EDS analyses confirm that Sr addition leads to the precipitation of Al_4Sr phase, which is consistent with the SEM observations. The possibility of the formation of metallic compounds can be predicted from the equilibrium phase diagram and the electronegativity of the two elements [16]. The difference in electronegativity between Sr and Al is higher than that between Mn and Al. Therefore, with increase of the Sr content, the Mn peak appears in Fig. 2. However, the

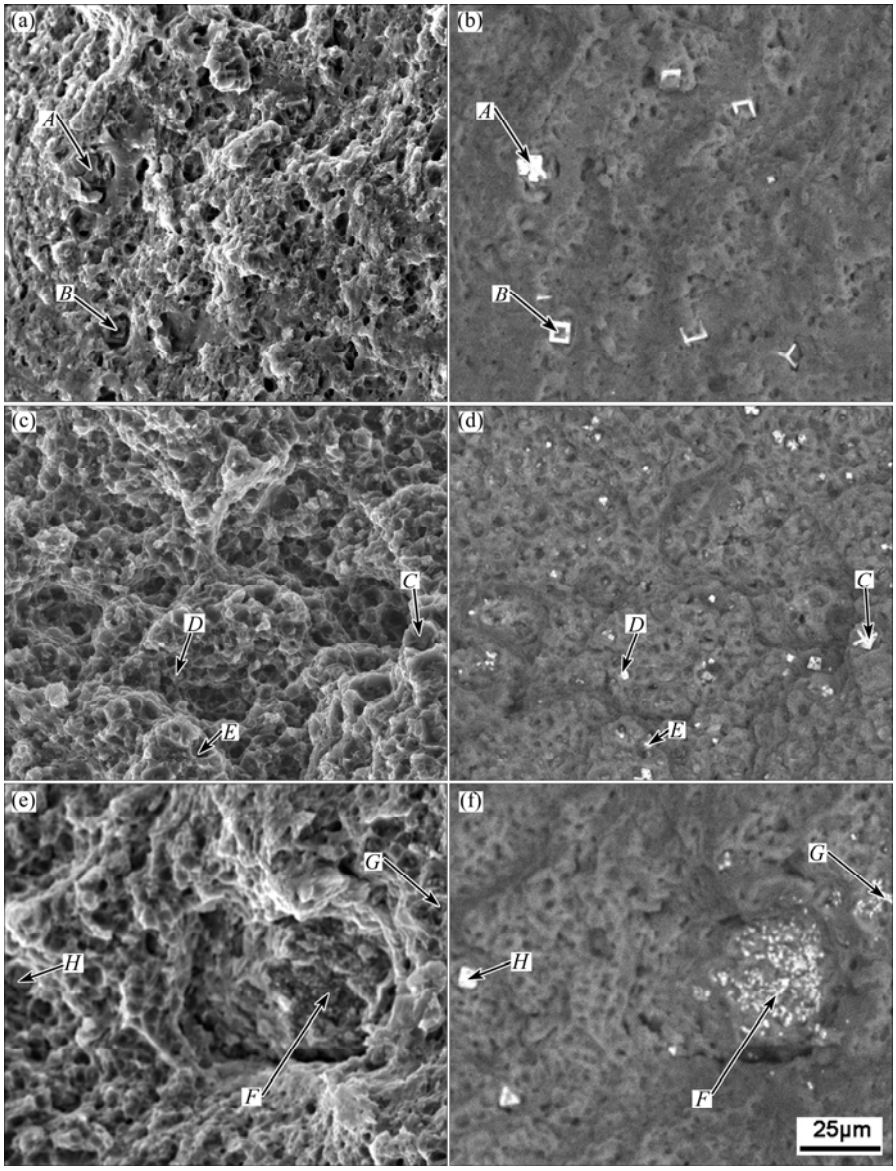

Fig. 7 Typical SEM images of SE morphology and BSE morphology of fracture surfaces of as-extruded alloys: (a, b) Mg−8Li−3Al−0.5Mn; (c, d) Mg−8Li−3Al−0.5Mn−0.5Sr; (e, f) Mg−8Li−3Al−0.5Mn−1.0Sr

Table 4 Element contents of different positions in Fig. 7 (mole fraction, %)

Position	O	Mg	Al	Mn	Sr
A	16.53	36.26	16.88	30.33	−
B	13.15	51.58	12.11	23.16	−
C	15.57	37.35	18.49	26.24	2.35
D	5.58	77.88	11.96	−	4.58
E	7.26	71.63	15.49	−	5.62
F	9.53	35.79	38.10	4.73	11.85
G	13.16	57.13	19.83	1.82	8.06
H	12.77	63.54	16.46	−	7.23

solid solubility of Sr in Mg is only approximately 0.11% (mass fraction). This value is significantly low for most Sr intermetallic forms existing in the alloy [17]. Furthermore, part of Sr added in the alloy combines with Mg to form Mg_2Sr.

The effect of Sr addition on the α-Mg phase of as-cast LAM830 alloy can be explained on the basis of growth restriction factor (GRF) [18].

$$\mathrm{GRF}=\sum_i m_i c_{0,i}(k_i-1) \quad (1)$$

where m_i is the slope of the liquidus line in the binary phase diagram; $c_{0,i}$ is the initial concentration of component I; and K_i is the equilibrium partition coefficient of component i. In general, GRF represents the ability to inhibit grain growth. The greater the value of GRF is, the stronger its ability is to inhibit grain growth. According to the binary phase diagrams of Mg−Sr alloy, m_{Sr}=−3.53, k_{Sr}=0.006, and $m_{Sr}(k_{Sr}-1)$=3.51 [19]. Substituting these values in Eq. (1), it can be seen that GRF increases with Sr content. Accordingly, the grain growth is inhibited with the increase of Sr content, realizing the goal of grain refinement.

Furthermore, the intermetallic compounds may play a key role in the efficiency of grain-refining. ZHANG et al [20,21] showed that an intermetallic compound could be used for the grain refinement of the metal matrix when the crystallographic mismatch of the close- or near-close-packed planes between the compound and the metal matrix is less than 10%. From the XRD results, the potential matching planes among Al_4Sr, Mg_2Sr, α-Mg and β-Li can be obtained. The mismatch values of these planes can also be determined through the definition method [22−24]. Table 5 shows the mismatch values of potential matching planes for Al_4Sr and Mg_2Sr compounds, and matrix α-Mg and β-Li phases, which are less than 10%.

Table 5 Mismatch values of potential matching planes for compounds and matrix

$Al_4Sr(004)$// α-Mg(002)	$Al_4Sr(004)$// α-Mg(100)	$Al_4Sr(112)$// α-Mg(002)	$Al_4Sr(112)$// α-Mg(100)
6.30%	0.33%	4.84%	1.70%
$Al_4Sr(213)$// β-Li(200)	$Mg_2Sr(103)$// α-Mg(100)	$Mg_2Sr(220)$// β-Li (200)	$Mg_2Sr(215)$// β-Li (211)
0.46%	6.66%	8.43%	3.71%

During the solidification (extrusion) process, Sr and its compounds could cause constitutional supercooling, thereby the grains of the as-cast alloys are refined. Consequently, the grains of get as-extruded alloys are refined. Besides, during extrusion, high melting compounds such as Al_4Sr can restrain dynamically recrystallized grain growth and refine the grains. The strengthening effects originating from the grain-size strengthening can be estimated from the Hall–Petch law:

$$\sigma_{ys} = \sigma_0 + kd^{-1/2} \quad (2)$$

where σ_{ys} is the yield strength of the alloys; σ_0 (11 MPa/μm^2) is the yield strength of pure Mg; k is a parameter determined for the polycrystalline material (0.28 MN·m$^{-3/2}$ for Mg); and d is the grain size [25]. From Figs. 1 and 4, it can be determined whether the grain size of the as-cast or as-extruded LAM830–0.75Sr alloys is the smallest among the alloys investigated in this study. Therefore, based on Eq. (2), it is possible to understand the reason for the higher strength of LAM830–0.75Sr alloys than other corresponding alloys.

When 0.25% Sr is added, the alloy strength decreases, which can be attributed to the following reasons. On one hand, the grain refining and solid-solution strengthening effects are weak after hot extrusion, especially for lower concentrations of Sr; On the other hand, addition of Sr in the alloy reacts with Al to form Al_4Sr. This weakens the solid-solution strengthening effects of Al [26]. The abovementioned factors are unfavorable for the mechanical properties of alloys. Both the strength and elongation of the as-extruded alloys decrease with 1% Sr addition. This is mainly because of the partial assembly of the secondary phase, as shown in Figs. 1(e) and 7(e, f). The combination of matrix and the large block of intermetallic compound is weak, so that the microcracks are easily formed between the matrix and intermetallic compound under serious stress concentration during the tension test. This ultimately leads to poor mechanical properties of LAM830−1.0Sr alloy.

5 Conclusions

1) The as-cast LAM830 alloy comprises α-Mg, β-Li, Al_2Mn_3 and $LiMgAl_2$ phases. Sr addition results in the formation of new blocky intermetallic compound distributed along the phase boundaries between α-Mg and β-Li phases with discontinuous network morphology. XRD and EDX analyses show that the precipitated compounds are Al_4Sr and Mg_2Sr.

2) The secondary dendrite arm spacing of the primary α-Mg phase can be refined with Sr addition. The secondary dendrite arm spacing of alloy with 0.75% Sr is the smallest.

3) The as-extruded LAM830−0.5Sr alloy exhibits an optimal elongation of 22.43%, which is increased by approximately 43.97% compared with that of as-extruded LAM830 alloy. The as-extruded LAM830−0.75Sr alloy shows an optimal tensile strength of 265.46 MPa, which is increased by approximately 19.38% compared with that of the alloy without Sr.

4) Fracture analysis of the as-extruded alloys reveals that the fracture in LAM830–0.5Sr alloy is the typical ductile fracture, and the interface of matrix and the secondary phases in Sr-containing alloys is strong. However, further increase in Sr content results in the partial assembly of the secondary phase, leading to poor ductility.

References

[1] WANG J, LIU R D, LUO T J, YANG Y S. A high strength and ductility Mg−Zn−Al−Cu−Mn magnesium alloy [J]. Materials & Design, 2013, 47: 746−749.

[2] ZHENG F Y, WU Y J, PENG L M, LI X W, FU P H, DING W J. Microstructures and mechanical properties of friction stir processed Mg−2.0Nd−0.3Zn−1.0Zr magnesium alloy [J]. Journal of Magnesium and Alloys, 2013, 1(2): 122−127.

[3] XIANG Q, WU R Z, ZHANG M L. Influence of Sn on microstructure and mechanical properties of Mg−5Li−3Al−2Zn alloys [J]. Journal of Alloys and Compounds, 2009, 477(1−2): 832−835.

[4] LEI B, LE Q C, ZHANG Z Q, CUI J Z, LI Q X. Effect of homogenization treatment on microstructure evolution and the distributions of RE and Zr elements in various Mg−Li−RE−Zr alloys [J]. Journal of Magnesium and Alloys, 2013, 1(2): 139−144.

[5] JIANG B, YIN H M, YANG Q S, LI R H, PAN F S. Effect of stannum addition on microstructure of as-cast and as-extruded Mg−5Li alloys [J]. Transactions of Nonferrous Metals Society of China, 2011, 21(11): 2378−2383.

[6] JACKSON R J, FROST P D. Properties and current applications of magnesium−lithium alloys [M]. Washington, DC: NASA SP, 1967.

[7] GOLMAKANIYOON S, MAHMUDI R. Microstructure and creep behavior of the rare-earth doped Mg−6Zn−3Cu cast alloy [J]. Mater Sci Eng A, 2011, 528(3): 1668−1677.

[8] PARK S S, BAE G T, KANG D H, JUNG I H, SHIN K S, KIM N J. Microstructure and tensile properties of twin-roll cast Mg−Zn−Mn−Al alloys [J]. Scripta Mater, 2007, 57(9): 793−796.

[9] ZHANG Z Y, PENG L M, ZENG X Q, DING W J. Effects of Cu and Mn on mechanical properties and damping capacity of Mg−Cu−Mn alloy [J]. Transactions of Nonferrous Metals Society of China, 2008, 18(S1): s55−s58.

[10] NGUYEN D N, MOTILAL M, MARIA F, DEOK S J. Effect of manganese additions on the corrosion behavior of an extruded Mg−5Al based alloy [J]. Journal of Alloys and Compounds, 2012, 542: 199−206.

[11] ERCAN K, MUSTAFA K. Effect of Mn additions on the microstructure and microhardness of as-cast and rapidly solidified Mg−5Ni−5Cu alloy [J]. Journal of Non-Crystalline Solids, 2013, 367: 70−81.

[12] YANG M B, PAN F S, CHENG R J, TANG A T. Comparation about efficiency of Al−10Sr and Mg−10Sr master alloys to grain refinement of AZ31 magnesium alloy [J]. J Mater Sci, 2007, 42(24): 10074−10079.

[13] WAN X F, SUN Y S, XUE F, BAI J, TAO W J. Effects of Sr and Ca on the microstructure and properties of Mg−12Zn−4Al−0.3Mn alloy [J]. Mater Sci Eng A, 2009, 508(1−2): 50−58.

[14] LIU T, WU S D, LI S X, LI P J. Microstructure evolution of Mg−14%Li−1%Al alloy during the process of equal channel angular pressing [J]. Mater Sci Eng A, 2007, 460: 499−503.

[15] WANG J, FU J W, DONG X G, YANG Y S. Microstructure and mechanical properties of as-cast Mg−Al−Sn−Y−Nd alloy [J]. Materials and Design, 2012, 36: 432−437.

[16] Metal Department of Zhongshang University. Physical and chemical constants of rare earth [M]. Beijing: Metallurgical Industry Press, 1978. (in Chinese)

[17] OKAMOTO H. Desk handbook: Phase diagrams for binary alloys [M]. 1st ed. OH: ASM International, 2000.

[18] TAMURE Y, KONO N, MOTEGI T. Grain refining mechanism and casting structure of Mg−Zr alloy [J]. Journal of Tapan Institute of Light Metals, 1998, 48: 185−189.

[19] LEE Y C, DAHLE A K, STJOHN D H. The role of solute in grain refinement of magnesium [J] Metallurgical and Materials Transactions A, 2000, 31(11): 2895−2905.

[20] ZHANG M X, KELLY P M, EASTON M A, TAYLOR J A. Crystallographic study of grain refinement in aluminum alloys using the edge-to-edge matching model [J]. Acta Materialia, 2005, 53(5): 1427−1438.

[21] ZHANG M X, KELLY P M, QIAN M, TAYLOR J A. Crystallography of grain refinement in Mg−Al based alloys [J]. Acta Materialia, 2005, 53(11): 3261−3271.

[22] LI R H, PAN F S, JIANG B, YIN H M, LIU T T. Effects of yttrium and strontium additions on as-cast microstructure of Mg−14Li−1Al alloys [J]. Transactions of Nonferrous Metals Society of China, 2011, 21(4): 778−783.

[23] JIANG B, QIU D, ZHANG M X, DING P D, GAO L. A new approach to grain refinement of an Mg−Li−Al cast alloy [J]. Journal of Alloys and Compounds, 2010, 492(1−2): 95−98.

[24] FU H M, QIU D, ZHANG M X, WANG H, KELLY P M, TAYLOR J A. The development of a new grain refiner for magnesium alloys using the edge-to-edge model [J]. Journal of Alloys and Compounds, 2008, 45(1−2): 390−394.

[25] YANG Y, PENG X D, WEN H M, ZHENG B L, ZHOU Y Z, XIE W D, LAVERNIA E J. Influence of extrusion on the microstructure and mechanical behavior of Mg−9Li−3Al−*x*Sr alloys [J]. Metallurgical and Materials Transactions A, 2013, 44(2): 1101−1113.

[26] CUI C L, WU L B, WU R Z, ZHANG J H, ZHANG M L. Influence of yttrium on microstructure and mechanical properties of as-cast Mg−5Li−3Al−2Zn alloy [J]. Journal of Alloys and Compounds, 2011, 509(37): 9045−9049.

Sr 含量对 Mg−Li−Al−Mn 合金显微组织及力学性能的影响

许天才[1]，彭晓东[1,2]，姜军伟[1]，谢卫东[1,2]，陈元芳[1,3]，魏国兵[1]

1. 重庆大学 材料科学与工程学院，重庆 400044；

2. 重庆大学 国家镁合金材料工程技术研究中心，重庆 400044；

3. 重庆理工大学 材料科学与工程学院，重庆 400050

摘　要：利用真空感应炉在氩气保护下，设计与制备 Mg−8Li−3Al−0.5Mn−*x*Sr (*x*=0~1.0)合金，并将其进行热挤压处理。分别研究合金铸态与挤压态显微组织和拉伸性能。结果表明：LAM830 合金主要含有 α-Mg，β-Li，Al_2Mn_3 和 $LiMgAl_2$ 相。在加入 Sr 后合金中出现 Al−Sr 析出相。Sr 对铸态合金 α-Mg 基体的二次枝晶臂有明显细化效果。经过热挤压处理的合金组织远优于铸态的合金组织。金属间化合物的含量与形态对合金力学性能的影响很大，其中挤压态的 LAM830−0.5Sr 具有最佳的伸长率(22.43%)，LAM830−0.75Sr 合金具有最佳的抗拉强度(265.46 MPa)。

关键词：镁锂合金；枝晶间距；Al_4Sr 相；力学性能

(Edited by Chao WANG)